

# Environment Semantics Aided Wireless Communications: A Case Study of mmWave Beam Prediction and Blockage Prediction

Yuwen Yang, Feifei Gao, Xiaoming Tao, Guangyi Liu and Chengkang Pan

**Abstract**—In this paper, we propose an environment semantics aided wireless communication framework to reduce the transmission latency and improve the transmission reliability, where semantic information is extracted from environment image data, selectively encoded based on its task-relevance, and then fused to make decisions for channel related tasks. As a case study, we develop an environment semantics aided *network architecture* for mmWave communication systems, which is composed of a semantic feature extraction network, a feature selection algorithm, a task-oriented encoder, and a decision network. With images taken from street cameras and user's identification information as the inputs, the environment semantics aided network architecture is trained to predict the optimal beam index and the blockage state for the base station. It is seen that without pilot training or the costly beam scans, the environment semantics aided network architecture can realize extremely efficient beam prediction and timely blockage prediction, thus meeting requirements for ultra-reliable and low-latency communications (URLLCs). Simulation results demonstrate that compared with existing works, the proposed environment semantics aided network architecture can reduce system overheads such as storage space and computational cost while achieving satisfactory prediction accuracy and protecting user privacy.

**Index Terms**—Semantic communications, channel semantics, environment semantics, deep learning, URLLC

## I. INTRODUCTION

As identified by Shannon and Weaver [1], communications can be categorized into three levels: i) transmission of symbols; ii) transmission of semantic information behind transmitted symbols; iii) effectiveness of semantic information interaction. In 1950s, Shannon focused on the first level and derived a rigorous mathematical theory of communications based on probabilistic models, yielding the famous Shannon capacity limit [2]. In the past decades, wireless communication systems based on the Shannon information theory have evolved from the first generation (1G) to the fifth generation (5G). Various advanced technologies, including massive multiple-input multiple-output (MIMO) [3], mmWave communications [4], and deep learning (DL) based communications [5], continuously promote the system capacity to Shannon capacity limit.

In particular, DL has been recognized as a promising candidate for beyond-5G (B5G) communications due to its remarkable capability of learning intricate inter-relationships hidden in massive data. Great progresses have been achieved by DL in physical layer communications such as channel estimation [6]–[9], data detection [10]–[12], channel feedback [13]–[15], and beamforming [16]–[18], etc. By either modifying or replacing conventional communication modules, these studies exploit deep neural networks (DNNs) to improve system accuracies or reduce computational complexities. Despite of continuously emerging DL based communication applications, the Shannon capacity limit is still the insurmountable upper bound.

Driven by the ambitious goals of the sixth generation (6G) and empowered by the development of artificial intelligence, a higher level communication paradigm, i.e., semantic communications, has been proposed very recently, which no longer focuses on accurately recovering the transmitted symbols but concerns on precisely recovering the meaning behind the transmitted symbols [19], [20]. The term “semantic information” refers to the information/meaning associated with the source signals. Semantic information exists in various signal modalities like texts, speeches, images, videos, and even random variables etc [21]–[24]. Studies on semantic communications in the area of computer vision (CV) and natural language processing (NLP) have attracted great attentions. The paradigm of semantic communications is to extract semantic information, transmit semantic information, and ensure semantic information being correctly interpreted by the receiver. Several recent works [25]–[28] have provided concrete examples of semantic text [25], [26], speech [27], and image [28] transmissions. In [25], the authors propose a DL based semantic communication architecture for text transmission, where the Transformer structure [29] is adopted in the semantic encoder/decoder. In the training process, the semantic accuracy and the system capacity are jointly optimized, while in the testing process the word-error-rate and the peak signal-to-noise ratio (PSNR) are used to measure the accuracy of the source information recovery. The corresponding simulations demonstrate the superiority of the semantic architecture over traditional approaches. Following the semantic communication architecture in [25], the work [26] introduces an adaptive circulation mechanism into the Transformer structure [29]. With the adaptive Transformer, the semantic communication system becomes more flexible to transmit sentences with different semantic information and exhibits better robustness over channel conditions. In [28], the authors propose a DL based

Y. Yang and F. Gao are with Institute for Artificial Intelligence Tsinghua University (THUI), State Key Lab of Intelligent Technologies and Systems, Beijing National Research Center for Information Science and Technology (BNRist), Department of Automation, Tsinghua University, Beijing, 100084, P. R. China (email: yyw18@mails.tsinghua.edu.cn, feifeigao@ieee.org).

X. Tao is with the Department of Electronic Engineering, Tsinghua University, Beijing, P.R. China, 100084 (email: taoxm@tsinghua.edu.cn).

G. Liu and C. Pan are with the China mobile communication research Institute, Beijing, China (e-mail: liuguangyi@chinamobile.com; panchengkang@chinamobile.com).

image semantic coding algorithm under a rate-perception-distortion optimization framework, which can achieve the state-of-the-art visually pleasing reconstruction and semantic preserving performance in the extreme low bit rate case.

In fact, all the existing semantics communication systems only utilize the semantics of source signals to enhance the information representation power of the transmission bits, which can be more precisely referred to as source-oriented semantic communications (SOSCs). The SOSC systems aim to promote the achieve rate reaching the Shannon capacity limit, which is consistent with the goal of enhanced mobile broad band (eMBB). Meanwhile, how to realize ultra-reliable and low-latency communications (URLLCs) is also an essential topic for the implementation of an efficient practical system. Since mmWave bands have abundant spectrum resources and support wider subcarrier spacing, mmWave communication systems can better meet low latency requirements in URLLCs. However, mmWave communication system is inherently unreliable due to its sensitivity to blockage and high penetration loss. To explore mmWave systems in URLLCs, the acquisitions of channel, interference, and blockage information are critical, especially for decisions like the beam switching or the base station (BS) hand-off.

Intrinsically, channels are determined by the wireless propagation environment, while the propagation environment can be captured by the images/visions from the cameras in cars or streets. Hence, one may extract the channel semantic information from environment images, named as environment semantics or channel semantics, to help channel related downstream tasks. By exploiting environment semantics, channel related downstream tasks could be accomplished without conventional channel estimation, which can significantly save the time and the computation cost related to the pilot training or the channel feedback, and even predict burst channel interference to improve the communication reliability. Actually, some works have already proposed to use environment images to help channel related downstream tasks, e.g., beam selection [30], channel covariance matrix estimation [31], and blockage prediction [32]. These vision based works demonstrate that channel information could be effectively attained from environment images to build communication connections without pilot overheads. However, original image usages for channel related tasks require expensive storage space, high computational cost, and huge energy consumption, which is unacceptable for the base stations (BSs) or users. Moreover, environment image usages may involve complex social issues such as user privacy, public safety, and management policies, especially when the third party cameras (e.g., the ubiquitous surveillance cameras) are employed to provide the environment images. Compared with directly utilizing environment images, operating with environment semantics naturally protects privacy. This is because that only the class and the layout information of objects are preserved in environment semantics, and the surface characteristics of objects are eliminated. Furthermore, environment semantics is associated with various objects, including key scatterers of propagation channels and objects that are irrelevant to propagation channels. By retaining channel relevant semantics and mitigating channel

irrelevant semantics, the system overheads such as storage space and computational cost could be also reduced. The environment semantics aided communication system focuses on exploring channel semantics hidden in environment images, and therefore can be regarded as channel-oriented semantic communications (COSCs).

In this paper, we propose a framework for COSCs, where environment semantics is extracted from environment images, selectively encoded based on its channel-relevance, and then fused to make decisions for specific channel related downstream tasks. To demonstrate the effectiveness of the proposed framework, we develop an environment semantics aided network architecture for mmWave beam prediction and blockage prediction as a case study. The environment semantics aided network architecture is composed of an environment semantics extraction network, a feature selection (FS) algorithm, a task-oriented encoder network, and a decision network. With images taken from street cameras, the environment semantics is obtained, selected, encoded, and then transmitted to BS. After fusing the encoded channel semantics and identification information of the target user, BS can obtain the predicted beam index and blockage state by the decision network. The environment semantics aided beam prediction can realize extremely low-latency without pilot training or the costly beam scans, while the environment semantics aided blockage prediction can support ultra-reliable communication links. Therefore, the proposed environment semantics aided framework offers extraordinary application values for URLLCs. Simulation results based on the autonomous driving and the ray-tracing channel simulators demonstrate the effectiveness of the proposed environment semantics aided communication framework, which further validates its great application potential in URLLCs.

The rest of this paper is organized as follows. The frameworks of COSCs and SOSCs are proposed in Section II. As a case study, the environment semantics aided network architecture for mmWave beam prediction and blockage prediction is developed in Section III. Numerical simulations are provided in Section IV. The main conclusions are given in Section V.

*Notation:* The bold and lowercase letters denote vectors; the notation  $(\cdot)^T$  denotes the transpose of a matrix or a vector; the notations  $\mathbb{C}^{m \times n}$  and  $\mathbb{R}^{m \times n}$  represent the  $m \times n$  complex and the  $m \times n$  real vector space, respectively; the notation  $\|\mathbf{x}\|_2$  denotes the  $L_2$  norm of  $\mathbf{x}$ ; the notation  $|\mathbf{x}|$  denotes the  $L_1$  norm of  $\mathbf{x}$  while  $|X|$  denotes the size of the set  $X$ .

## II. SOURCE SEMANTICS AND CHANNEL SEMANTICS

In this section, we will introduce SOSCs, and then propose a framework of environment semantics aided communication systems as a representative instance of COSCs. A communications system working with both SOSCs and COSCs will be named as a generalized semantics communications systems. We will then heuristically analyze the source semantics and channel semantics.

### A. Existing Semantic Communication Systems: SOSCs

Fig. 1 illustrates the frameworks of a classical (the upper part) and an existing semantic (the bottom part) com-

munication systems. In a classical communication system, signals with various modalities are first compressed by a source encoder to save transmission cost. Then, the designed redundancies are added by a channel encoder to combat physical channel noises in transmission links, and the received signals experience the inverse process in the receiver side. Unlike classical communications whose goal is to ensure each transmitted bit being correctly received, the SOSC systems [25]–[28] aim to guarantee the meaning behind the transmitted bits, i.e., the semantic information of the transmitted signals, being correctly understood by the receiver. Details about the modules of the existing semantic communication systems are given in the following.

**Semantic encoder** extracts semantic features from the source signals and compresses them to save the transmission cost. Next, the compressed semantic features go through a channel encoder and are transmitted over physical channels.

**Semantic decoder** interprets the received semantic features and recover the original source signals, i.e., conducting the inverse process of the semantic encoder.

**Background knowledge base (BKB)** is the prerequisite of semantic communication systems, which can be independently established or interactively shared by the transmitter and the receiver. The semantic encoder extracts semantic features based on the background knowledge at the transmitter, while the semantic decoder interprets semantic features and restores the original source signals based on the background knowledge at the receiver. The BKBs can learn from previous signal data and periodically update with the gradual progress of communications. Naturally, BKBs are different in various contexts. For example, high-frequency words in business and medical scenarios are different, and therefore the corresponding BKBs contain different semantic corpora. Moreover, BKBs should have different formats for signals in various modalities, e.g., text, image, and speech, etc. Besides, BKBs at the transmitter and the receiver might be different due to cognitive bias or belated sharing.

**Semantic noise** comes from semantic ambiguity of received signals or mismatches between the BKBs at the transmitter and the receiver, resulting in semantic errors in the interpretation and recovery processes. Note that the physical channel noise in transmission environments might lead to symbol errors of the received signals, which can also cause semantic errors.

### B. Environment Semantics Aided Communication System: COSCs

The framework of the environment semantics aided communication system is displayed in the middle part of Fig. 1, where semantic information is extracted from environment images for channel related downstream tasks, e.g., beam prediction, blockage prediction, and codebook designs, etc. We refer the semantic information extracted from environment images as environment semantics or the channel semantics, which naturally protects user privacy by eliminating the surface characteristics of objects and preserving only the class and the layout information of objects. Since the environment semantics aided communication system exploits the channel semantics

hidden in the environment images to assist channel related downstream tasks, it can be regarded as an instance of COSCs.

To illustrate the idea, suppose the goal of environment semantics aided communication systems is to predict the parameter  $Y$  from a set of multimodal observations/samples, including environment images [33]. Here  $Y$  can be the beam index/vector in beam prediction tasks, the blockage flag in blockage prediction tasks, the codebook in codebook design tasks, or the channel covariance matrix in channel covariance matrix estimation tasks, etc. We refer features extracted from other relevant modalities as *auxiliary features*, which can help to identify target users or provide extra system information. Denote the universal set of the extracted features as  $X_{\text{uni}}$ . By utilizing FS methods, the most efficient feature set could be selected from  $X_{\text{uni}}$ . Then, the task-oriented encoder maps  $X$  into  $\tilde{X}$  to save system overheads (e.g., storage space, transmission delay, and energy consumption, etc). The compressed semantic feature set  $\tilde{X}$  is sent to the fusion module for further decisions in channel related downstream tasks.

### C. Analyses of Source Semantics and Channel Semantics

Signals and channels are the two major components of communication systems. Existing semantic communication systems [25]–[28] are SOSCs that focus on the semantics of the source signals to enhance the representation capacity of transmitted bits. The proposed environment semantics aided communication system belongs to COSCs that extract the channels semantics from multimodal data like environment images to assist the accomplishment of channel related downstream tasks without pilot training. In other words, SOSCs improve the representation capacity of transmitted bits by utilizing the source signal semantics, i.e., pursuing the goal of eMBB. In contrast, COSCs improve the transmission efficiency by exploiting the channel semantics hidden in multimodal data, i.e., targeted at the requirements of URLLCs. In the environment semantics aided communication system, channel semantics refers to the shape and classes of channel relevant scatterers, which can be obtained from the environment images. Besides, the proposed environment semantics aided communication system is a concrete realization of task-oriented communications, where the module interactions are carried out to accomplish a specific task while the information not strictly relevant to the task would be mitigated. [34].

## III. CASE STUDY OF CHANNEL SEMANTICS: MMWAVE BEAM PREDICTION AND BLOCKAGE PREDICTION

In this section, we develop an environment semantics aided network architecture for mmWave beam prediction and blockage prediction to meet requirements of URLLCs as a case study.

### A. System Model

Consider a massive MIMO system, where a BS is equipped with  $N_t \gg 1$  antennas in the form of uniform linear array (ULA) and serves multiple single-antenna users. The received frequency domain signal of a user on the  $k$ -th subcarrier is

$$r[k] = \mathbf{h}^T[k] \mathbf{w}s[k] + \varepsilon[k], \quad (1)$$

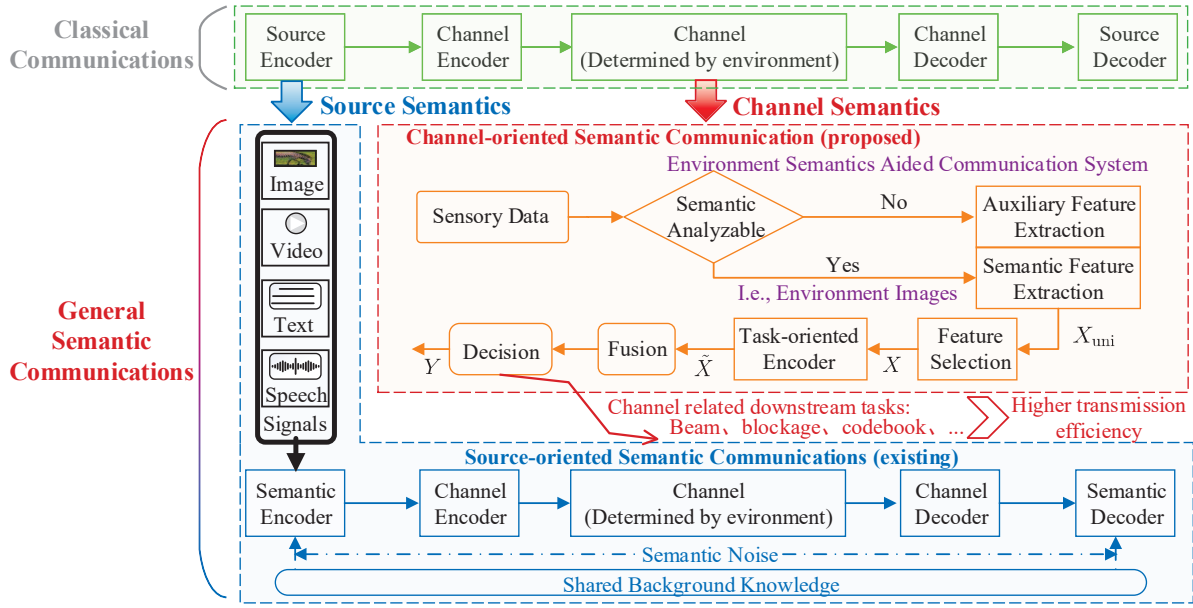


Fig. 1. Frameworks of a classical (the upper part), an existing semantic (the bottom part), and an environment semantics aided (the middle part) communication systems. The environment semantics aided and the existing semantic communication systems are the instances of COSCs and SOSCs, respectively.

where  $r[k] \in \mathbb{C}^{1 \times 1}$  is the received signal,  $s[k] \in \mathbb{C}^{1 \times 1}$  is the transmit signal,  $\mathbf{w} \in \mathbb{C}^{N_t \times 1}$  is the transmit beamforming vector, and  $\varepsilon[k] \sim \mathcal{CN}(0, \sigma_\varepsilon^2)$  is the additive white Gaussian noise. Moreover,  $\mathbf{h}[k] \in \mathbb{C}^{M \times 1}$  is the downlink channel that can be written as [35]

$$\mathbf{h}[k] = \sum_l \alpha_l e^{-j2\pi f_{D,k} \tau_l + j\phi_l} \mathbf{a}(\theta_{az}^l, \theta_{el}^l), \quad (2)$$

where  $f_{D,k}$  is the frequency of the  $k$ -th downlink subcarrier, while  $\alpha_l$ ,  $\phi_l$ , and  $\tau_l$  are the attenuation, phase shift, and delay of the  $l$ -th path, respectively. In addition,  $\mathbf{a}(\theta_{az}^l, \theta_{el}^l)$  is the array manifold vector<sup>1</sup> defined as

$$\mathbf{a}(\theta_{az}^l, \theta_{el}^l) = \begin{bmatrix} 1, e^{j\varpi \sin(\theta_{el}^l) \cos(\theta_{az}^l)}, \dots \\ \dots, e^{j\varpi(M-1) \sin(\theta_{el}^l) \cos(\theta_{az}^l)} \end{bmatrix}^T, \quad (3)$$

where  $\varpi = 2\pi d f_{D,k} / c$ ,  $d$  is the antenna spacing,  $c$  is the speed of light, and  $\{\theta_{az}^l, \theta_{el}^l\}$  is the {azimuth, elevation} angle of arrival. Assume the beamforming vector  $\mathbf{w}$  is selected from the beam codebook  $\mathcal{W}$ , where  $M_{bm} = |\mathcal{W}|$  is the codebook size. The achievable transmission rate corresponding to the beam vector  $\mathbf{w}$  can be written as

$$\text{Rate}_{\mathbf{w}} = \frac{1}{K} \sum_{k=1}^K \log_2 \left( 1 + \frac{P_k}{\sigma^2} |\mathbf{h}^T[k] \mathbf{w}|^2 \right), \quad (4)$$

where  $P_k = E[|s[k]|^2]$  is the power of the transmitted signal<sup>2</sup>. The optimal beamforming vector can be obtained by

maximizing the transmission rate, i.e.,

$$\mathbf{w}^{\text{opt}} = \arg \max_{\mathbf{w} \in \mathcal{W}} \text{Rate}_{\mathbf{w}}. \quad (5)$$

In fact, the beamforming vector  $\mathbf{w}$  is designed to concentrate the transmitter power on a narrow beam to compensate for the high penetration loss of mmWaves. To obtain the optimal beamforming vector  $\mathbf{w}^{\text{opt}}$ , conventional algorithms need to estimate accurate channel information by extensive downlink pilot training, thus leading to unacceptable time delay especially for massive MIMO systems. Besides, exhaustively searching on the a large codebook also greatly increases the time delay, which makes it impractical to apply conventional algorithms to URLLCs. In the meantime, based on field measurements [36], the channel power is generally concentrated in the first few paths, especially the line-of-sight (LOS) path. Therefore, LOS link blockages caused by obstacles would significantly reduce the achievable transmission rate, and even lead to link disconnections. To ensure the link reliability of mmWave communications, the prediction of future link blockages is critical to beam/BS switching decisions.

## B. Problem Formulation

As indicated in Eq. (2), millimeter massive MIMO channels have sparse structures associated with the parameters such as attenuations, phase shifts, and delays, etc. Naturally, these channel parameters can be regarded as one type of semantic information. However, from an intrinsical perspective, wireless channels are determined by the propagation paths or more straightforward by the key scatters in propagation environment, e.g., vehicles or roads. Therefore, there exists channel related semantic information in corresponding environment images that could be extracted to improve the channel related

<sup>1</sup>When other types of antenna arrays are adopted, the array manifold vector should be changed accordingly. Note that the proposed network architecture is not limited by specific antenna array shape, and therefore is applicable for array with arbitrary geometry.

<sup>2</sup>To simplify the notation, we drop the sub-carrier index  $k$  in the rest of the paper, e.g., replacing  $\mathbf{r}[k]$ ,  $\mathbf{h}_u(f_{D,k})$ , and  $\mathbf{s}[k]$  with  $\mathbf{r}$ ,  $\mathbf{h}(f_D)$ , and  $\mathbf{s}$ , respectively.

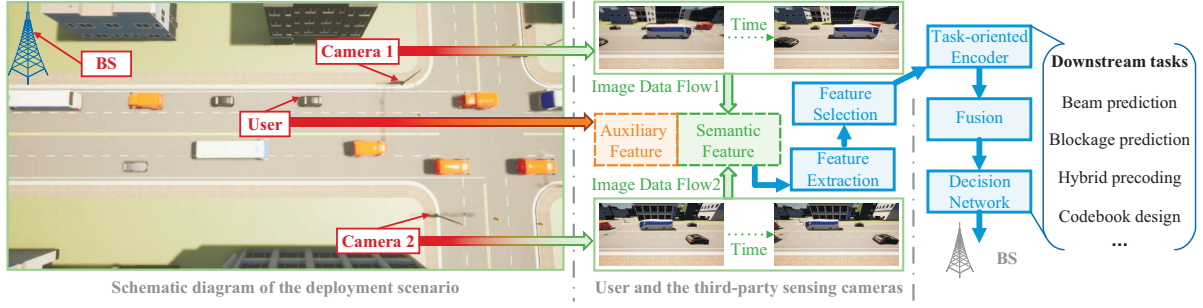


Fig. 2. The overall diagram of the environment semantics aided communication system. Here two cameras are schematically installed in the deployment scenario. In fact, the number and positions of the cameras can be set according to practical conditions and demands, which will not affect the algorithm design.

tasks, e.g., the beam prediction, blockage prediction, hybrid precoding, and codebook design, etc.

Suppose that cameras, i.e., the sensing devices installed on both sides of streets, can capture image data flows to assist BS in channel related tasks. As shown in Fig. 2, different cameras can provide image data from different perspectives, thus avoiding the target user being blocked by other vehicles nearby. Since images from cameras are municipal infrastructure data, which involve complex social issues such as user privacy, public safety, and management policies, etc, they should not be directly sent to the fusion center for communication services. By extracting environment semantics from images, the surface characteristics of buildings, vehicles, or roads, etc, are eliminated, while only the class and the layout information of objects are preserved. Therefore, environment semantics is naturally more private than original images, and facilitates potential new privacy transmission protocols. Meanwhile, user's identification information, such as locations, historical beam indexes, or other predetermined information that could be used to distinguish users, should also be sent to the fusion center in a secure and private way<sup>3</sup>. We refer the features extracted from users' identification information and environment semantics from cameras as auxiliary and semantic features, respectively. Raw multimodal data from communication or sensing devices are first transformed into auxiliary or semantic features, and then selectively encoded by the task-oriented encoder. After fusing the encoded features from the target user and the cameras on streets, optimal decisions can be obtained by the designed network at BS.

### C. Environment Semantics Aided Network Architecture for Beam Prediction and Blockage Prediction

Fig. 3 displays the diagram of the environment semantics aided network architecture for beam prediction and blockage prediction, consisting of the environment semantics extraction network, the FS algorithm, the task-oriented encoder, and the decision network. Specifically, the environment semantics extraction network is deployed independently at each camera

to extract the environment semantics from the corresponding environment images. The output of the environment semantics extraction network is the segmentation map, i.e., the pixel-wise category labels of the environmental semantic concepts (e.g., "road", "vehicle", "trafficlight", and "sky", etc). After multiplying the segmentation map by the corresponding zero-masks, one can obtain maps of various environmental semantic concepts, as shown in the lower left quarter of Fig. 3. We refer a map of each environmental semantic concept as an instance of one semantic feature. The universal feature set  $X_{\text{uni}} \triangleq \{X_{\text{uni},v} | v = 1, \dots, V_{\text{uni}}\}$  contains both the semantic features from environment images and the auxiliary features from users' identification information, where  $V_{\text{uni}} = |X_{\text{uni}}|$  denotes the size of  $X_{\text{uni}}$ . Note that many types of user's identification information, such as locations, historical beam indexes, or other predetermined information, could all be added to  $X_{\text{uni}}$  for further selection. In this work, we adopt the location as an example. Then, we utilize the FS algorithm to select the optimal feature sets, i.e.,

$$X_{\text{bm}} \triangleq \{X_{\text{bm},v} | v = 1, \dots, V_{\text{bm}}, X_{\text{bm},v} \in X_{\text{uni}}\}$$

and

$$X_{\text{bl}} \triangleq \{X_{\text{bl},v} | v = 1, \dots, V_{\text{bl}}, X_{\text{bl},v} \in X_{\text{uni}}\},$$

from  $X_{\text{uni}}$  for beam prediction and blockage prediction, where  $V_{\text{bm}}$  and  $V_{\text{bl}}$  are the sizes of  $X_{\text{bm}}$  and  $X_{\text{bl}}$ , respectively. Since the user's identification information is necessary to distinguish the target user from other possible users, the user location would definitely be retained by the FS algorithm as the auxiliary feature for both beam prediction and blockage prediction<sup>4</sup>. For clarify, we denote the location as the feature  $X_{\text{bm},1} \triangleq X_{\text{bl},1}$ . Hence,  $\{X_{\text{bm},v}\}_{v=2}^{V_{\text{bm}}}$  and  $\{X_{\text{bl},v}\}_{v=2}^{V_{\text{bl}}}$  are the semantic features selected from the environment semantics for beam prediction and blockage prediction, respectively. The task-oriented encoder is composed of the auxiliary, the semantic-beam, and the semantic-blockage modules. The decision network includes the blockage-prediction and the beam-prediction modules. With  $X_{\text{bm}}$  as the input, the three modules, i.e., the auxiliary, the semantic-beam, and the beam-prediction modules, are jointly trained to predict the beam. With  $X_{\text{bl}}$  as

<sup>3</sup>If restricted, the feature extraction could be independently implemented by terminal devices without communications with subsequent communication tasks. More details about how to strictly protect user privacy involve specific device transmission protocols and encryption methods, which are possibly left as future work.

<sup>4</sup>When more types of users' identification information are involved, which type of users' identification information is retained depends on the FS algorithm.



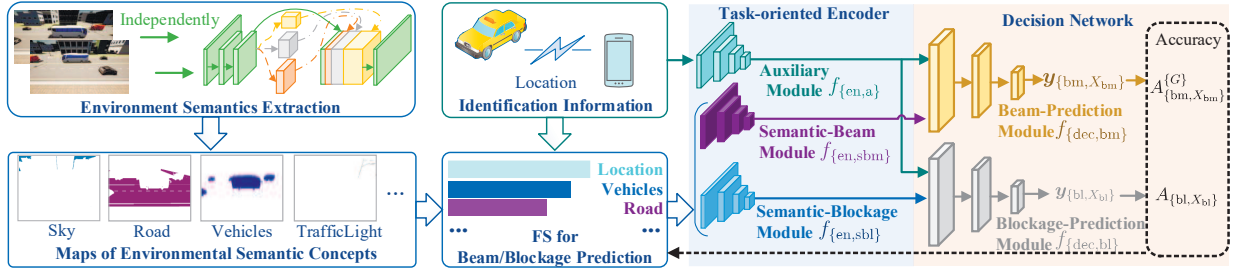


Fig. 3. Diagram of the environment semantics aided network architecture for beam prediction and blockage prediction.

the input, the three modules, i.e., the auxiliary, the semantic-blockage, and the blockage-prediction modules, are jointly trained to predict the blockage. Since pilot training and costly beam scans are unnecessary, the environment semantics aided network architecture is expected to realize low-latency beam prediction and blockage prediction to ensure efficient and reliable mmWave communication links, so as to fulfilling the goal of URLLCs.

In the following, we will present the environment semantics extraction network, followed by the structures of above-mentioned modules. Then, the FS algorithm for beam prediction and blockage prediction are presented respectively. Lastly, the overall training steps of the environment semantics aided network architecture for beam prediction and blockage prediction are provided.

1) *The environment semantics extraction network:* In semantic coded transmission work [28], a semantic-perceptual loss defined by the semantic segmentation network PSPNet [23] is adopted for image compression and reconstruction, which is experimentally demonstrated to yield better reconstruction performance than common pixel-level losses at the same transmission bit rate. The work [28] also validates that the reconstructed images suffering less semantic information losses could achieve better performance in downstream tasks like object detection. Inspired by this, we utilize PSPNet to extract environment semantics from environment images, as shown in Fig. 4. Inheriting from the well-known ResNet [37], PSPNet is composed of a serial of basic residue blocks, and each residue block is sequentially stacked by several convolution, batch normalization (BatchNorm), and ReLu layers. We refer the outputs of hidden layers as the feature maps, and mark them with serial numbers in Fig. 4 for illustration convenience. The main difference of PSPNet compared with ResNet is the pyramid pooling module, where the 3-rd feature map first goes through three pooling layers with different down-sampling rates in parallel. Then, the three down-sampled feature maps independently and successively go through a convolution and a BatchNorm layers, obtaining three feature maps with different pyramid scales, i.e., the {4,5,6}-th feature maps. Next, the {4,5,6}-th feature maps are up-sampled by bilinear interpolations such that they can be concatenated together with the 3-rd feature map as the final pyramid pooling global feature, i.e., the 7-th feature map. Note that the number of residue blocks, convolutional filters, and pyramid levels can all be adjusted on demand. The principle of the pyramid

pooling module is that 1) feature maps with smaller scales has larger sizes of receptive fields<sup>5</sup>; 2) layers with larger receptive fields could learn more about the global features of images while layers with smaller receptive fields could learn more about the local features of images; 3) the pyramid pooling module could learn a comprehensive feature of images by fusing feature maps with varying scales. Denote the input image as  $\mathbf{g} \in \mathbb{R}^{3 \times H \times W}$ , where “3” denotes the RGB channels,  $H$  is the image height, and  $W$  is the image width. The label and the output of PSPNet are  $\hat{\mathbf{c}} \in \mathbb{R}^{M_{\text{con}} \times H \times W}$  and  $\mathbf{c} \in \mathbb{R}^{H \times W}$ , respectively, where  $M_{\text{con}}$  is the number of semantic feature categories, and the  $(i, j)$ -th entry of  $\mathbf{c}$  is the category label of the environmental semantic concept at the pixel coordinate  $(i, j)$ , i.e.,  $\mathbf{c}(i, j) = 0, \dots, M_{\text{con}} - 1$ . The loss function of the PSPNet is given by

$$f_{\{\text{L}_{\text{psp}}\}} = -\frac{1}{HW} \sum_{i,j} \log \left( \frac{\exp(\hat{\mathbf{c}}(\mathbf{c}(i, j), i, j))}{\sum_{m=0}^{M_{\text{con}}-1} \exp(\hat{\mathbf{c}}(m, i, j))} \right). \quad (6)$$

By using the ADAM algorithm to minimize  $f_{\{\text{L}_{\text{psp}}\}}$  until the convergence, the segmentation map can be obtained by

$$\mathbf{c}_{\text{map}} = \arg \max_{m=0, \dots, M_{\text{con}}-1} \hat{\mathbf{c}}(m, i, j). \quad (7)$$

The extraction accuracy of the environment semantics is then given by

$$A_{\text{PSP}} = \frac{\sum_{i,j} \sum_{n=1}^{N_{\text{tot}}} \mathbb{1}(\mathbf{c}_{\text{map}}^{(n)}(i, j) = \mathbf{c}^{(n)}(i, j))}{HWN_{\text{tot}}}, \quad (8)$$

where the superscript  $(n)$  denotes the  $n$ -th sample,  $\mathbb{1}$  is the indicator function, and  $N_{\text{tot}}$  is the total number of testing samples. The accuracy  $A_{\text{PSP}}$  measures the accuracy of the environment semantics extraction. After obtaining the segmentation map, i.e.,  $\mathbf{c}_{\text{map}}$ , the environment semantics such as “road”, “vehicle”, “trafficlight”, “pedestrian”, “sky”, and “building”, etc, can be easily separated by multiplying zero-masks.

2) *The auxiliary module:* With the location as the input<sup>6</sup>, the auxiliary module is composed of several fully connected (FC) blocks, and each FC block is sequentially stacked by an

<sup>5</sup>The receptive field is the locations in deeper layers correspond to the locations in the input image they are path-connected to.

<sup>6</sup>In this example work, we can prejudice that the user location would be the input of the auxiliary-module. When more types of users' identification information are involved, the design of the auxiliary module would be more complex and depends on which type of users' identification information is chosen by the FS algorithm.

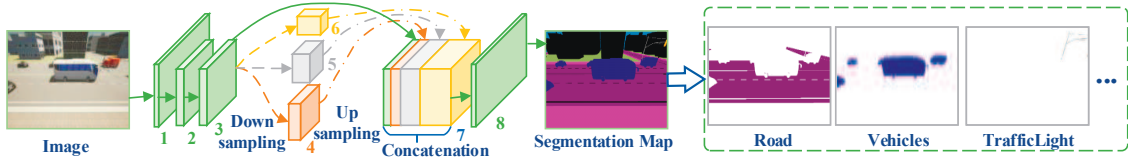


Fig. 4. Illustration of the environment semantics extraction. A green cuboid represents a feature map output by a basic residue block. The number next to the cuboid is the marked index of the feature map but does not necessarily correspond to the actual number of blocks. Cuboids in other colors represent feature maps of different size in the pyramid pooling module. Notice that cuboids with smaller side areas typically are thicker in the horizontal direction. This is because that when images are down sampled, we tend to increase the filter number to avoid information loss, which is also a common trick in computer vision.

FC, a BatchNorm, and a ReLu layers. Denote the mathematical function of the auxiliary module as  $f_{\{en,a\}}$  for future use. Although we adopt the same network structure of the auxiliary module for both beam prediction and blockage prediction, the specific network parameters of the auxiliary module would be trained independently for beam prediction and blockage prediction.

3) *The semantic-beam module:* With the selected semantic features  $\{X_{bm,v}\}_{v=2}^{V_{bm}}$  as the input, the semantic-beam module is built by stacking several convolution-blocks, and each convolution-block contains a convolution, a BatchNorm, and a Relu layers in sequence. The output size of the semantic-beam module can be changed by adjusting the number of convolution blocks, the number of filters in the convolution layer, or the down-sampling rate of the pooling layer. Denote the mathematical function of the semantic-beam module as  $f_{\{en, sbm\}}$  for future use.

4) *The semantic-blockage module:* With the selected semantic features  $\{X_{bl,v}\}_{v=2}^{V_{bl}}$  as the input, the semantic-blockage module has similar structure with the semantic-beam module, i.e., stacked by several convolution blocks. Denote the mathematical function of the semantic-blockage module as  $f_{\{en, sbl\}}$  for future use.

5) *The beam-prediction module:* The input of the beam-prediction module can be given as

$$\mathbf{x}_{\{bm, X_{bm}\}} = [f_{\{en,a\}}(X_{bm,1}), f_{\{en, sbm\}}(\{X_{bm,v}\}_{v=2}^{V_{bm}})]. \quad (9)$$

With  $\mathbf{x}_{\{bm, X_{bm}\}}$  as the input, the beam-prediction module is composed of several FC, dropout, and Relu layers. Define the mathematical function of the beam-prediction module as  $f_{\{dec, bm\}}$ . Then, the output of the beam-prediction module is

$$\mathbf{y}_{\{bm, X_{bm}\}} = f_{\{dec, bm\}}(\mathbf{x}_{\{bm, X_{bm}\}}). \quad (10)$$

The cross entropy loss is adopted for beam prediction, which is given by

$$f_{\{Lbm, X_{bm}\}} = -\log \left( \frac{\exp(\mathbf{y}_{\{bm, X_{bm}\}}[y_{\{bm, lab\}}])}{\sum_{m=1}^{M_{bm}} \exp(\mathbf{y}_{\{bm, X_{bm}\}}[m])} \right), \quad (11)$$

where  $y_{\{bm, lab\}}$  is the beam label. The auxiliary, the semantic-beam, and the beam-prediction modules are jointly trained by applying adaptive moment estimation (ADAM) algorithm [38] to minimize  $f_{\{Lbm, X_{bm}\}}$  until the convergence. Denote the Top- $G$  beam-index set of the  $n$ -th testing sample as  $Y_{\{G, X_{bm}\}}^{(n)}$ , which contains the indices corresponding to  $G$  maximum values of the output vector  $\mathbf{y}_{\{bm, X_{bm}\}}^{(n)}$ . Then, the Top- $G$  beam

prediction accuracy can be obtained by

$$A_{\{G, X_{bm}\}} = \sum_n^{N_{tot}} \mathbb{1}(y_{\{bm, lab\}}^{(n)} \in Y_{\{G, X_{bm}\}}^{(n)}) / N_{tot}. \quad (12)$$

Denote the Top- $G$  beam-vector set as  $\mathcal{W}_{\{G, X_{bm}\}}^{(n)}$ , where each beam vector in  $\mathcal{W}_{\{G, X_{bm}\}}^{(n)}$  is selected from the codebook  $\mathcal{W}$  according to the beam index set  $Y_{\{G, X_{bm}\}}^{(n)}$ . The transmission rate corresponding to  $Y_{\{G, X_{bm}\}}^{(n)}$  can be written as

$$\text{Rate}_{Y_{\{G, X_{bm}\}}^{(n)}} = \max_{\mathbf{w} \in \mathcal{W}_{\{G, X_{bm}\}}^{(n)}} \text{Rate}_{\mathbf{w}}. \quad (13)$$

Define the transmission rate ratio (TRR) of the Top- $G$  beam as the ratio between the transmission rate corresponding to  $Y_{\{G, X_{bm}\}}^{(n)}$  and the optimal transmission rate corresponding to the beam  $\mathbf{w}^{opt}$  in Eq. (14), i.e.,

$$\text{TRR}_{\{G, X_{bm}\}} = \frac{1}{N_{tot}} \sum_n^{N_{tot}} \frac{\text{Rate}_{Y_{\{G, X_{bm}\}}^{(n)}}}{\text{Rate}_{\mathbf{w}^{opt}}}. \quad (14)$$

It should be mentioned that with the Top- $G$  beam-vector set  $\mathcal{W}_{\{G, X_{bm}\}}^{(n)}$ , BS only needs to scan  $G$  times to obtain the optimal beam. In this way, the environment semantics aided network architecture offers an ideal initial beam search range, and thus significantly reduces the delay caused by beam scans.

6) *The blockage-prediction module:* The input of the blockage-prediction module can be written as

$$\mathbf{x}_{\{bl, X_{bl}\}} = [f_{\{en,a\}}(X_{bl,1}), f_{\{en, sbl\}}(\{X_{bl,v}\}_{v=2}^{V_{bl}})]. \quad (15)$$

With  $\mathbf{x}_{\{bl, X_{bl}\}}$  as the input, the blockage-prediction module is composed of several FC, dropout, and Relu layers. Define the mathematical function of the blockage-prediction module as  $f_{\{dec, bl\}}$ . Then, the output of the blockage-prediction module is

$$y_{\{bl, X_{bl}\}} = \sigma(f_{\{dec, bl\}}(\mathbf{x}_{\{bl, X_{bl}\}})), \quad (16)$$

where  $\sigma(z) = 1/(1 + e^{-z})$  is the sigmoid function. We adopt the binary cross entropy loss for blockage prediction, which is given by

$$f_{\{Lbl, X_{bl}\}} = y_{\{bl, lab\}} \log y_{\{bl, X_{bl}\}} + (1 - y_{\{bl, lab\}}) \log (1 - y_{\{bl, X_{bl}\}}), \quad (17)$$

where  $y_{\{bl, lab\}}$  is the blockage label. The auxiliary, the semantic-blockage, and the blockage-prediction modules are jointly trained by ADAM algorithm to minimize  $f_{\{Lbl, X_{bl}\}}$  until the convergence. In the testing stage, the blockage accuracy

can be obtained by

$$A_{\{bl, X_{bl}\}} = \sum_n^{N_{tot}} \mathbb{1}(y_{\{bl, X_{bl}\}}^{(n)} = y_{\{bl, lab\}}^{(n)}) / N_{tot}. \quad (18)$$

7) *FS for beam prediction*: For simplicity, we adopt the Top-1 beam prediction accuracy as the optimization objective of FS. Based on Eq. (12), the Top-1 beam prediction accuracy with the feature set  $X$  can be calculated by

$$A_{\{1, X_{bm}\}} = \sum_n^{N_{tot}} \mathbb{1}(y_{\{1, X_{bm}\}}^{(n)} = y_{\{bm, lab\}}^{(n)}) / N_{tot}, \quad (19)$$

where  $y_{\{1, X_{bm}\}}^{(n)}$  is the predicted Top-1 beam of the  $n$ -th sample, i.e.,

$$y_{\{1, X_{bm}\}}^{(n)} = \arg \max_{m=0, \dots, M_{bm}-1} \mathbf{y}_{\{bm, X_{bm}\}}^{(n)}[m]. \quad (20)$$

Originated from the SFFS algorithm, the proposed FS algorithm takes the universal feature set  $X_{uni}$  as the input and then outputs the selected subset  $X_{bm}$ , where the mapping mechanism from the feature set  $X_{bm}$  to the Top-1 beam prediction accuracy  $A_{\{1, X_{bm}\}}$  serves as the optimization objective. Denote the selected subset at the  $i$ -th iteration as  $X_{bm}^{(i)}$ . The history feature set  $X_{\{bm, hist\}}$  contains the history iterations of the selected subset. We initialize both  $X_{bm}^{(0)}$  and  $X_{\{bm, hist\}}$  as empty sets. The FS algorithm can be divided into two alternate steps, i.e., Step 1 and Step 2, until a termination criterion is satisfied. Step 1 aims to find the most significant feature  $x^+$  among the unselected features, i.e., the feature leading to the best accuracy increase for  $X_{bm}^{(i)}$ :

$$x^+ \leftarrow \arg \max_{x \in X_{uni} - X_{bm}^{(i)}} A_{\{1, X_{bm}^{(i)} + x\}}. \quad (21)$$

After successively updating  $X_{bm}^{(i+1)}$ ,  $X_{\{bm, hist\}}$ , and  $i$  by

$$X_{bm}^{(i+1)} \leftarrow X_{bm}^{(i)} + x^+, \quad (22)$$

$$X_{\{bm, hist\}} \leftarrow \{X_{\{bm, hist\}}, X_{bm}^{(i)}\}, \quad (23)$$

and  $i \leftarrow i + 1$ , respectively, we go over to Step 2 with the goal to remove the least significant feature in  $X_{bm}^{(i)}$ . In Step 2, if there exists one feature in  $X_{bm}^{(i)}$  that has a negative contribution to the accuracy, i.e., satisfying

$$\max_{x \in X_{bm}^{(i)}} A_{\{1, X_{bm}^{(i)} - x\}} > A_{\{1, X_{bm}^{(i)}\}}, \quad (24)$$

then we will remove the feature  $x^-$  that results in the maximum accuracy drop, i.e., obtaining  $x^-$  by

$$x^- \leftarrow \arg \max_{x \in X_{bm}^{(i)}} A_{\{1, X_{bm}^{(i)} - x\}}. \quad (25)$$

After successively updating  $X_{bm}^{(i+1)}$  and  $i$  by

$$X_{bm}^{(i+1)} \leftarrow X_{bm}^{(i)} - x^-, \quad (26)$$

and  $i \leftarrow i + 1$ , we go back to check the condition Eq. (24). If Eq. (24) is not satisfied, then it indicates any feature in  $X_{bm}^{(i)}$  has a positive contribution to the accuracy. In this case, we will come to Step 1 to select the most significant feature  $x^+$  in the feature set  $X_{uni} - X_{bm}^{(i)}$ . In Step 1, when  $X_{bm}^{(i)}$  has appeared in history feature set  $X_{\{bm, hist\}}$ , the iteration will

---

**Algorithm 1:** FS algorithm for beam prediction

---

**Input:** Universal feature set  $X_{uni} \triangleq \{X_{uni, v} | v = 1, \dots, V_{uni}\}$   
**Output:** Selected feature set  $X_{bm} \triangleq \{X_{bm, v} | v = 1, \dots, V_{bm}, X_{bm, v} \in X_{uni}\}$

- 1 Initialize feature set  $X_{bm}^{(0)} \leftarrow \emptyset$
- 2 history feature set  $X_{\{bm, hist\}} \leftarrow \emptyset$ ;  $i = 0$
- 3 **Step 1: (Inclusion)**
- 4 **if**  $X_{bm}^{(i)} \notin X_{\{bm, hist\}}$  **then**
- 5  $x^+ \leftarrow \arg \max_{x \in X_{uni} - X_{bm}^{(i)}} A_{\{1, X_{bm}^{(i)} + x\}}$ ;  $X_{bm}^{(i+1)} \leftarrow X_{bm}^{(i)} + x^+$
- 6  $X_{\{bm, hist\}} \leftarrow \{X_{\{bm, hist\}}, X_{bm}^{(i)}\}$
- 7  $i \leftarrow i + 1$
- 8 **go to Step 2**
- 9 **else**
- 10 **Output**  $X_{bm} \leftarrow X_{bm}^{(i)}$
- 11 **end**
- 12 **Step 2: (Conditional Exclusion)**
- 13 **if**  $\max_{x \in X_{bm}^{(i)}} A_{\{1, X_{bm}^{(i)} - x\}} > A_{\{1, X_{bm}^{(i)}\}}$  **then**
- 14  $x^- \leftarrow \arg \max_{x \in X_{bm}^{(i)}} A_{\{1, X_{bm}^{(i)} - x\}}$ ;  $X_{bm}^{(i+1)} \leftarrow X_{bm}^{(i)} - x^-$
- 15  $i \leftarrow i + 1$
- 16 **go to Step 2**
- 17 **else**
- 18 **go to Step 1**
- 19 **end**

---

enter an infinite same loop, i.e., the feature added in Step 1 will be removed in Step 2, which means we cannot find a feature set that outperforms  $X_{bm}^{(i)}$  in terms of the beam prediction accuracy. Therefore, the algorithm ends and outputs  $X_{bm} \leftarrow X_{bm}^{(i)}$ . The detailed steps of the FS algorithm for beam prediction are given in **Algorithm 1**. In fact, other termination criterion could also be adopted. For instance, to limit the number of select features, i.e.,  $|X_{bm}|$  being no more than  $V_{max}$ , we could replace Line 4 of **Algorithm 1** with “**if**  $X_{bm}^{(i)} \notin X_{\{bm, hist\}}$  **and**  $|X_{bm}^{(i)}| < V_{max}$  **then**”. In this way, **Algorithm 1** can output the optimal feature subset  $X_{bm}$  with specified size.

8) *FS for blockage prediction*: The FS algorithm for blockage prediction aims to select the optimal feature set  $X_{bl}$ . The detailed steps of the FS algorithm for blockage prediction is the same with that for beam prediction except that its optimization objective is replaced by  $A_{\{bl, X_{bl}\}}$ , as shown in **Algorithm 2**.

9) *The overall training steps of the environment semantics aided network architecture*: The overall implementation steps can be given as follows:

- i) Train the environment semantics extraction network at each camera end, i.e., using ADAM algorithm to minimize Eq. (6) until the convergence. The extraction accuracy of the environment semantics is calculated by Eq. (8).
- ii) Apply **Algorithm 1** to select the optimal feature set  $X_{bm}$  from the universal feature set  $X_{uni}$ . For each iterated feature set, the auxiliary, the semantic-beam, and the beam-prediction modules would be jointly retrained by minimizing Eq. (11) until the convergence. The Top-1 beam prediction accuracy corresponding to the iterated



**Algorithm 2:** FS algorithm for blockage prediction

---

**Input:** Universal feature set  $X_{\text{uni}} \triangleq \{X_{\text{uni},v} | v = 1, \dots, V_{\text{uni}}\}$   
**Output:** Selected feature set  $X_{\text{bl}} \triangleq \{X_{\text{bl},v} | v = 1, \dots, V_{\text{bl}}, X_{\text{bl},v} \in X_{\text{uni}}\}$

- 1 Initialize feature set  $X_{\text{bl}}^{(0)} \leftarrow \emptyset$
- 2 history feature set  $X_{\{\text{bl},\text{hist}\}} \leftarrow \emptyset$ ;  $i = 0$
- 3 **Step 1: (Inclusion)**
- 4   **if**  $X_{\text{bl}}^{(i)} \notin X_{\text{hist}}$  **then**
- 5      $x^+ \leftarrow \arg \max_{x \in X_{\text{uni}} - X_{\text{bl}}^{(i)}} A_{\{\text{bl}, X_{\text{bl}}^{(i)} + x\}}$ ;  $X_{\text{bl}}^{(i+1)} \leftarrow X_{\text{bl}}^{(i)} + x^+$
- 6      $X_{\{\text{bl},\text{hist}\}} \leftarrow \{X_{\{\text{bl},\text{hist}\}}, X_{\text{bl}}^{(i)}\}$
- 7      $i \leftarrow i + 1$
- 8     **go to Step 2**
- 9   **else**
- 10     **Output**  $X_{\text{bl}} \leftarrow X_{\text{bl}}^{(i)}$
- 11   **end**
- 12 **Step 2: (Conditional Exclusion)**
- 13   **if**  $\max_{x \in X_{\text{bl}}^{(i)}} A_{\{\text{bl}, X_{\text{bl}}^{(i)} - x\}} > A_{\{\text{bl}, X_{\text{bl}}^{(i)}\}}$  **then**
- 14      $x^- \leftarrow \arg \max_{x \in X_{\text{bl}}^{(i)}} A_{\{\text{bl}, X_{\text{bl}}^{(i)} - x\}}$ ;  $X_{\text{bl}}^{(i+1)} \leftarrow X_{\text{bl}}^{(i)} - x^-$
- 15      $i \leftarrow i + 1$
- 16     **go to Step 2**
- 17   **else**
- 18     **go to Step 1**
- 19   **end**

---

feature set is tested by Eq. (19).

- iii) Save and fix the parameters of the auxiliary, the semantic-beam, and the beam-prediction modules corresponding to the optimal feature set  $X_{\text{bm}}$ .
- iv) Apply **Algorithm 2** to select the optimal feature set  $X_{\text{bl}}$  from the universal feature set  $X_{\text{uni}}$ . For each iterated feature set, the auxiliary, the semantic-blockage, and the blockage-prediction modules would be jointly retrained by minimizing Eq. (17) until the convergence. The blockage accuracy corresponding to the iterated feature set is tested by Eq. (18).
- v) Save and fix the parameters of the auxiliary, the semantic-blockage, and the blockage-prediction modules corresponding to the optimal feature set  $X_{\text{bl}}$ . Note that the initialization, the training, and the storage of the auxiliary module in Step iv)-Step v) are all independent with those in Step ii)-Step iii).
- vi) The cameras only send the selected environment semantics, i.e.,  $X_{\text{bm}} \cup X_{\text{bl}}$ , to the task-oriented encoder. Then, BS obtains the predicted Top- $G$  beam and blockage by the decision network.

**Remark:** Compared with the pervious vision based works [30]–[32] that directly utilize environment image data to assist channel related tasks, the environment semantics aided network architecture enjoys two main benefits:

- Environment semantics are extracted from environment images for subsequent data processing, which can not only protect user privacy especially in the case of using the third part cameras, but also reduce the system overheads (e.g., storage space and computational cost) brought by channel-irrelevant information.

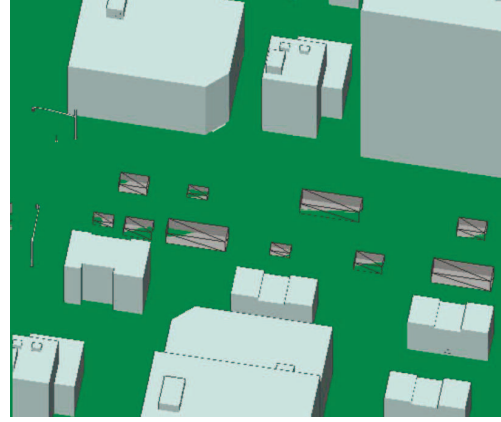


Fig. 5. A partial view of the synchronization simulation in the Wireless Insite simulator. To save the cost of art designs, we utilize simple cubes to model the buildings and the vehicles in Wireless Insite and ignore the surface details of these elements. The losses in surface details have limited influences on the channels, which will not affect the reliability of simulations.

- Channel semantics is extracted from environment images, which reveals the key scatterers associated with channel propagation paths and further provides an interpretable insight into the joint communication and sensing systems.

## IV. SIMULATION RESULTS

### A. Simulation Setup

1) *Environment modeling:* The autonomous driving simulator CARLA [39] is utilized to simulate the street traffic environment, including the street landscape, vehicles, and cameras, etc. Vehicles in the deployment scenario are randomly chosen from the three types, i.e., the car ( $3.71 \times 1.79 \times 1.55\text{m}^3$ ), the van ( $5.20 \times 2.61 \times 2.47\text{m}^3$ ), and the bus ( $11.08 \times 3.25 \times 3.33\text{m}^3$ ). Then, we utilize the traffic simulation software SUMO [40] to control the speed and trajectory of all the vehicles. A partial view of the street traffic environment is shown in the left of Fig. 2.

2) *Scene image and semantic label generation:* As shown in Fig. 2, two cameras are set at 5m on both sides of the street, both orienting towards the street. The two cameras keep taking images as vehicles cross the street. Fortunately, the CARLA simulator can generate the corresponding semantic label for each images taken by cameras. There are 20 classes of environmental semantic concepts, including “building”, “fence”, “pedestrian”, “pole”, “roadline”, “sidewalk”, “vegetation”, “vehicle”, “wall”, “trafficsign”, “sky”, “ground”, “bridge”, “railtrack”, “trafficlight”, “static”, “dynamic”, “water”, “terrain”, and “unlabeled”. In particular, the concept “static” refers to the elements that are immovable, e.g., fire hydrants, fixed benches, and bus stops, etc. The concept “dynamic” refers to the elements that are susceptible to move over time, e.g., wheelchairs, animals, and buggies, etc. The concept “unlabeled” refers to the elements that have not been categorized. By collecting the {image, semantic label} pairs and splitting them to the training and the testing datasets, the semantic feature extraction network PSPNet [23] could be trained to produce the corresponding environment semantics.

TABLE I  
THE NETWORK PARAMETERS FOR THE BEAM PREDICTION AND BLOCKAGE PREDICTION

Module	Layer	Kernel	Stride	Filter/Neuron	Output Shape
Auxiliary	BatchNorm	/	/	3	3
	(FC-BatchNorm-ReLu) $\times 2$	/	/	256,16	16
Semantic-beam	(Conv-BatchNorm-ReLu) $\times 2$	3, 3	4, 2	32, 16	$16 \times 40 \times 80$
	AvgPool	3	2	/	$16 \times 20 \times 40$
	(Conv-BatchNorm-ReLu) $\times 2$ <Residual>	3, 3	4, 1	8, 8	$8 \times 5 \times 10$
	(Conv-BatchNorm-ReLu) $\times 2$ <Residual>	3, 3	1, 1	8, 8	$8 \times 5 \times 10$
Beam-prediction	(FC-BatchNorm-ReLu)	/	/	512	512
	Dropout	Rate: 0.1			512
	FC	/	/	64	64
		/	/	1	1
Semantic-blockage	(Conv-BatchNorm-ReLu)	3	2	16	$16 \times 40 \times 80$
	AvgPool	3	2	/	$16 \times 20 \times 40$
	(Conv-BatchNorm-ReLu) $\times 2$ <Residual>	3, 3	4, 1	8, 8	$8 \times 5 \times 10$
Blockage-prediction	(FC-BatchNorm-ReLu)	/	/	64	64
	Dropout	Rate: 0.1			64
	FC	/	/	1	1
		/	/	1	1

### 3) Channel, blockage label, and beam label generation:

To obtain the channels of users in vehicles, we synchronize the street traffic environment in CARLA with the 3D ray-tracing simulator Wireless InSite [35] at each moment that cameras take images, which ensures that the images taken by the two cameras exactly correspond to the channels. Since one image may contain several vehicles or users, we also record the location of the target user, to form the uniquely identified sample pair of the two environment images, the location, and the channel. Fig. 5 displays a partial view of the synchronization simulation in the Wireless Insite simulator, where the buildings and the sizes/locations/orientations of vehicles in Wireless Insite are exactly the same as that in CARLA at each image shooting moment. The carrier frequency is 28 GHz, the number of OFDM subcarriers is 128, and the BS is equipped with 64 antennas. After setting the transceiver antennas at the corresponding locations, the ray-tracing simulator shoots thousands of rays in all directions from the transmitter and records the strongest 20 paths that reach the receiver, obtaining the corresponding channel parameters, i.e.,  $\{\alpha_l, \phi_l, \tau_l, \theta_{az}^l, \theta_{el}^l\}$ , and further obtaining the channels using Eq. (2). The blockage labels can be obtained according to whether there exists a LOS path among the strongest 20 paths during the future time period between two image shootings. Each time slot is 50ms. Unless otherwise specified, the blockage prediction is to predict the next future time slot, i.e., blockage state in next 50ms. Following Eq. (5), the corresponding beam labels can be obtained by exhaustively searching on the codebook. Here we adopt the discrete fourier transformation codebook as an example.

4) *Network parameters:* The network structure of the feature extraction network follows the work [23], except that the input and the output dimensions are adjusted according to the shapes of the images and the semantic labels generated by CARLA. Moreover, various network scales, including ResNet-18, ResNet-34, ResNet-50, and ResNet-100 [37], are respectively adopted and trained on the datasets in Section IV-A2. The network parameters for the auxiliary, the semantic-beam, the semantic-blockage, the beam-prediction, and the blockage-prediction modules are given in Tab. I, where “-” represents

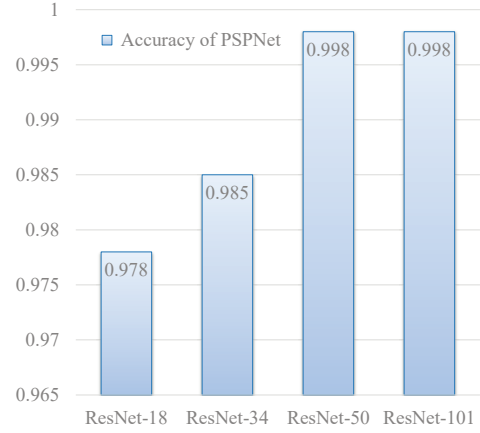


Fig. 6. The prediction accuracy of PSPNet, i.e., the accuracy of the environment semantics extraction, trained on datasets in Section IV-A2.

sequential stacking, “ $(\cdot) \times 2$ ” represents that the layers inside  $(\cdot)$  are sequentially stacked twice, the numbers split by “,” represents the parameters for adjacent convolution or FC layers, “<Residual>” represents the residual connection between the adjacent convolutional layers, and “Conv” is the abbreviation of “convolution”. The initial learning rate of the ADAM optimizer is 0.001, and the batch size is 128.

### B. Performance of the Environment Semantics Extraction

We adopt PSPNet to extract the environment semantics from environment images, which implies that the prediction accuracy of PSPNet, i.e.,  $A_{PSP}$ , is the accuracy of the environment semantics extraction. Fig. 6 exhibits the prediction accuracies of PSPNet versus the network scales. The accuracy of PSPNet improves as the network scale increases, and the accuracy saturates when the network scale reaches that of ResNet-50. The work [23] presents the accuracy of PSPNet on the ADE20K dataset [41], which is much lower than that on the datasets generated by CARLA. This is because that the number of semantic concepts to be classified in the ADE20K dataset is 150, which is much larger than that in our datasets, i.e.,

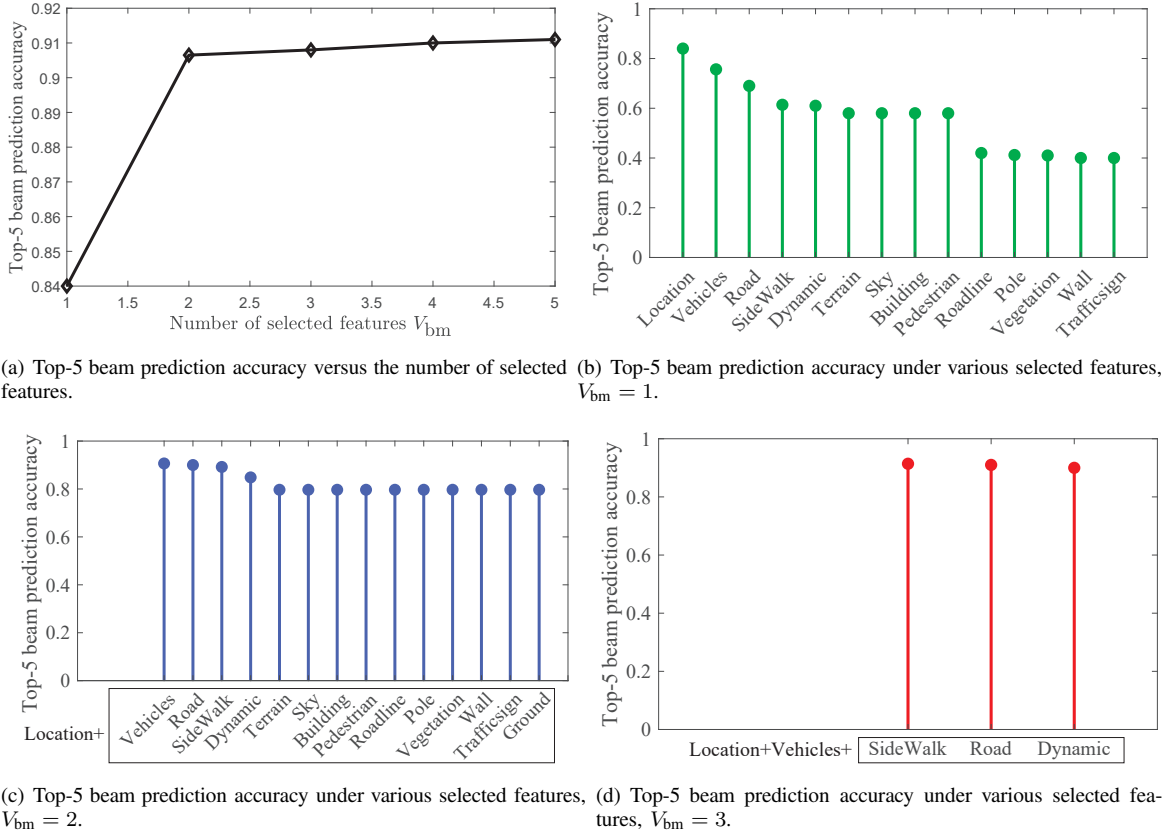


Fig. 7. The Top-5 beam prediction accuracy  $A_{\{5, X_{bm}\}}$  under various selected feature sets.

20. Therefore, the classification task for the ADE20K dataset is harder than that for our datasets. This indicates that the accuracy of the semantic feature extraction could be further improved if we could remove unimportant semantic features and further reduce the number of categories to be classified.

### C. Performance of FS for Beam Prediction and Blockage Prediction

Fig. 7 displays the Top-5 beam prediction accuracy  $A_{\{5, X_{bm}\}}$  under various feature sets selected by **Algorithm 1**. Fig. 7(a) plots the Top-5 beam prediction accuracy versus the number of selected features  $V$ , where the Top-5 beam prediction accuracy is obtained through the execution of **Algorithm 1**. More specifically, the Top-5 beam prediction accuracy at  $V_{bm} = v$  can be determined by

$$\arg \max_{X_{bm} \in X_{\{bm, hist\}}, |X_{bm}|=v} A_{\{5, X_{bm}\}}.$$

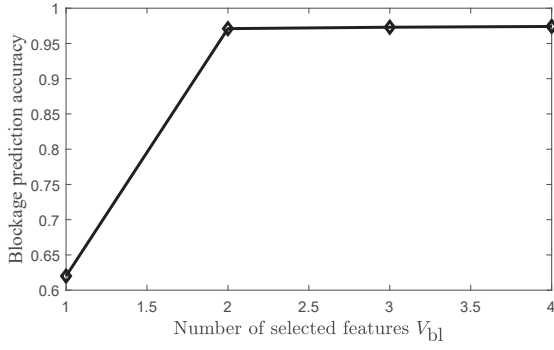
The Top-5 beam prediction accuracy improves as  $V_{bm}$  increases, while the accuracy gain is less than 0.01 when  $V_{bm}$  is larger than 3, which implies that three features are efficient enough for beam prediction. Fig. 7(b)-Fig. 7(d) present the Top-5 beam accuracies under various selected feature sets with  $V_{bm} = 1, 2$ , and 3, respectively, where the feature names are listed in descending order along the  $x$ -axis according to the corresponding accuracies. In Fig. 7(b), only one feature is utilized to predict the beam. The location yields the highest accuracy among all the features. This is because that the

location is the user's identification information, which is essential to distinguish the target user from other possible users<sup>7</sup>. The reason that other features like the vehicle still yield higher accuracies than random predictions is due to the limited concurrent users within the same image. In Fig. 7(c), two features are used to predict the beam, and one of them is the location. It can be seen that the three environment semantic concepts, i.e., "vehicle", "road", and "sidewalk", lead to the highest beam prediction accuracy. In Fig. 7(d), three features are utilized to predict the beam, and two of them are the location and the vehicle. The feature set {location, vehicle, sidewalk} can achieve the highest accuracy, which conforms to the intuition that the vehicles provide the information of users' directions and the possible obstacles, while sidewalks offer the information of street layouts.

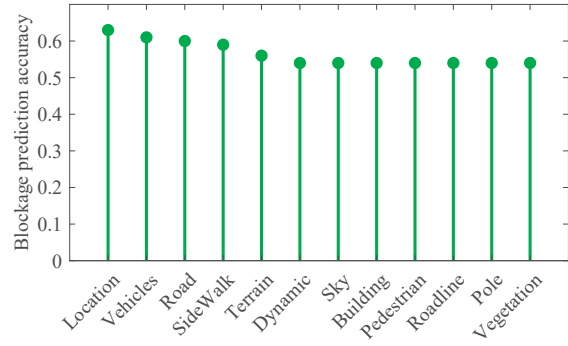
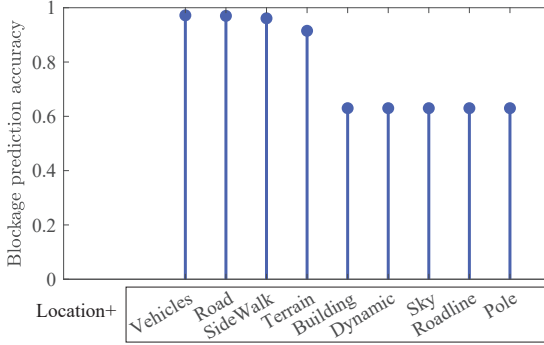
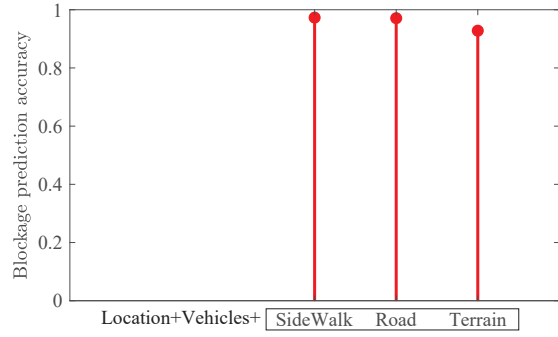
Fig. 8 displays the blockage prediction accuracy  $A_{\{bl, X_{bl}\}}$  under various feature sets selected by **Algorithm 2**. Fig. 8(a) plots the blockage prediction accuracy versus the number of selected features  $V_{bl}$ , where the blockage prediction accuracy at  $V_{bl} = v$  can be obtained by

$$\arg \max_{X_{bl} \in X_{\{bl, hist\}}, |X_{bl}|=v} A_{\{bl, X_{bl}\}}.$$

<sup>7</sup>The accuracy performance associated with the location also explains that location based works are popular [30]–[32]. In fact, other user's identification information, such as historical beam indices or other predetermined information, could also be used to distinguish the target user from other possible users. Therefore, the location based prediction is only a special case of the environment semantics aided communication system.



(a) Blockage prediction accuracy versus the number of selected features.

(b) Blockage prediction accuracy under various selected features,  $V_{bl} = 1$ .(c) Blockage prediction accuracy under various selected features,  $V_{bl} = 2$ .(d) Blockage prediction accuracy under various selected features,  $V_{bl} = 3$ .Fig. 8. The blockage prediction accuracy  $A_{\{bl, X_{bl}\}}$  under various selected feature sets.TABLE II  
ENVIRONMENT SEMANTICS ANALYSES

Environmental semantic concept	Accuracy contribution
Vehicles, Road, Sidewalk	Critical
Dynamic, Terrain	Moderate
Sky, Building, Pedestrian, Roadline, Pole, Vegetation, Wall, Ground, Bridge, Rail-track, Trafficlight, Water, Fence, Static	Negligible

It can be observed that two features are efficient enough for blockage prediction. Fig. 8(b)-Fig. 8(d) present the blockage prediction accuracies under various selected feature sets with  $V_{bl} = 1, 2$ , and  $3$ , respectively, where the feature names are listed in descending order along the  $x$ -axis according to the corresponding accuracies. Similar with Fig. 7, the feature set {location, vehicle, sidewalk} can achieve the highest accuracy. This validates that the feature set {location, vehicle, sidewalk} are the most significant features for channel related tasks, and other unselected semantic features have lower relevancy with channels.

Based on the results of Fig. 7 and Fig. 8, we divide the environmental semantic concepts into three levels of accuracy contributions, i.e., critical, moderate, and negligible, as shown in Tab. II. Obviously, the environmental semantic concepts “vehicles”, “road”, and “sidewalk” are the most critical features due to their contributions to the beam prediction and

TABLE III  
BEAM PREDICTION AND BLOCKAGE PREDICTION ACCURACIES WITH VARIOUS INPUTS

Input	Top-5 beam	Blockage
Original images	$0.910 \pm 0.091$	$0.971 \pm 0.088$
All environment semantics	$0.914 \pm 0.042$	$0.974 \pm 0.036$
{Vehicles, Road, Sidewalk}	$0.914 \pm 0.020$	$0.974 \pm 0.018$

blockage prediction. Therefore, the three environmental semantic concepts “vehicles”, “road”, and “sidewalk” can be interpreted as the most significant channel semantics, and other unselected semantic features have lower relevancy with the channels. For beam prediction, as shown in Fig. 7(c) and Fig. 7(d), “road” is more effective than “sidewalk” for  $V_{bm} = 2$  but is less effective than “sidewalk” for  $V_{bm} = 3$ . To understand the phenomenon, one can glean some indications in the right part of Fig. 4, where the shapes of “road” and “vehicles” are complementary, which implies that the better accuracy of “road” for  $V_{bm} = 2$  owns to its high dependency on “vehicles”, while the gain of “road” would be weakened for  $V_{bm} = 3$  where “vehicles” has been selected. When “vehicle” has been selected, “sidewalk” could offer extra beam prediction accuracy gains. Moreover, “dynamic” has moderate contributions to the beam prediction accuracy. This is because that “dynamic” objects in the road may change the shape of “vehicles”, and the acquisition of “dynamic” can modify the

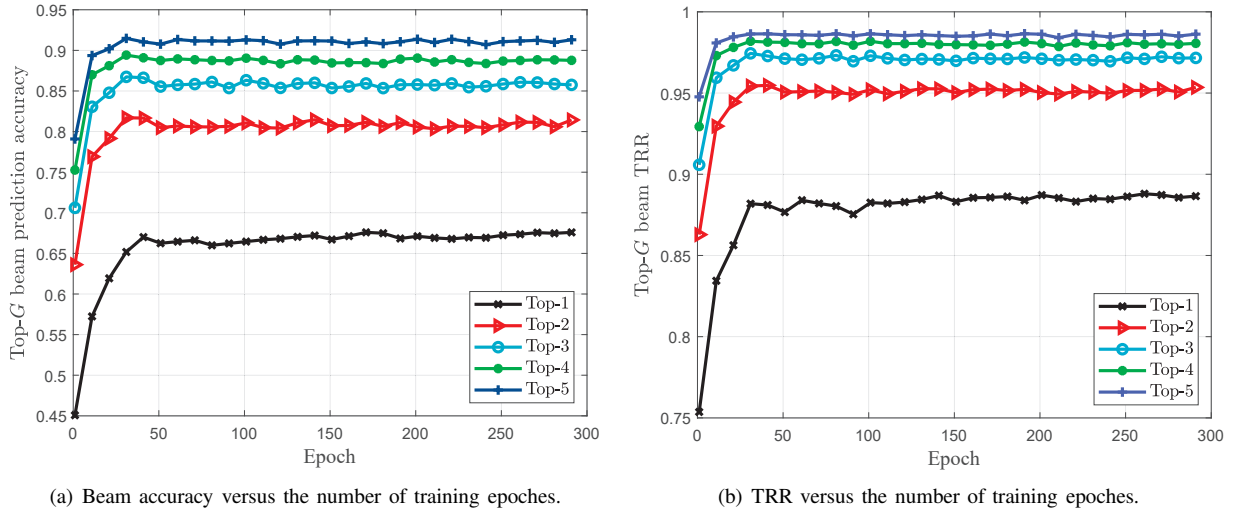


Fig. 9. The beam prediction accuracy (a) and the TRR (b) of the Top-G beam versus the number of training epoches.

TABLE IV  
BLOCKAGE PREDICTION ACCURACY VERSUS FUTURE TIME SLOTS

Time slots	1	6	11	16	21	26	31	36
$A_{\{bl, X_{bl}\}}$	0.9741	0.966	0.951	0.94	0.929	0.922	0.901	0.882

shape distortion, yielding noticeable contributions to the beam prediction accuracy. For blockage prediction, as shown in Fig. 8(c) and Fig. 8(d), the accuracy gain brought by the third feature sidewalk is marginal. This indicates that the environmental semantic concept “vehicles” is sufficient for blockage prediction, and blockage prediction is less sensitive to other environmental semantic concepts than beam prediction. This is because that the beam vector is highly related to various scatterers in environments while the blockage state is only related to the obstacle in the LOS path.

Tab. III compares the beam prediction and blockage prediction accuracies with various inputs, i.e., original images, all environment semantics, and the selected channel semantics set  $\{\text{location, vehicle, sidewalk}\}$ . The overall network structures for original images and all environment semantics are the same with those for the selected channel semantics, and the only difference is that the network input has been replaced by the original images and the segmentation maps, respectively. It can be observed that the channel semantics set is much sparse than the environment semantics set, but is informative enough to obtain almost the same prediction accuracy, which also demonstrates that the proposed FS algorithm can significantly compress the original image flows while preserve the most informative features. Furthermore, the standard deviations of the selected channel semantics set are smaller than those of original images and all environment semantics. This is because irrelevant semantics or fine image details expand the input feature space, making available samples sparser and more dissimilar, which results in a network more easier to overfit and generate unstable predictions. Therefore, the proposed environment semantics aided network architecture cannot only reduce system overheads brought by channel-irrelevant infor-

mation, but also improve the prediction robustness.

#### D. Performance of Top-G Beam Prediction

Fig. 9 depicts the beam prediction accuracy and the TRR of the Top-G beam versus the number of training epoches, where the feature set  $\{\text{location, vehicle, sidewalk}\}$  is adopted. It can be seen that the task-oriented encoders and decision network converge when the number of epoches is larger than 50. As shown in Fig. 9(a), the Top-1 beam prediction accuracy reaches 66%, and the Top-5 beam prediction accuracy reaches 91%. As shown in Fig. 9(b), the TRR of Top-1 beam reaches 88%, and the TRR of Top-5 beam reaches 98%. These results demonstrate the effectiveness of the proposed environment semantics aided network architecture.

#### E. Performance of Blockage Prediction Versus Future Time Slots

Tab. IV displays the blockage prediction accuracies versus future time slots, where each time slot is 50ms. For each recorded time slot point, i.e., 6, 12,  $\dots$ , 36, the network would be retrained with the corresponding future blockage labels. It can be seen that the blockage prediction accuracy is higher than 90% for future 30 time slots, i.e., 1.5s, which demonstrates the effectiveness of the proposed environment semantics aided network architecture.

## V. CONCLUSION

In this paper, we propose a framework for environment semantics aided wireless communications to improve the transmission efficiency and protect the user privacy. We also developed an environment semantics aided network architecture for mmWave beam prediction and blockage prediction



as a case study. Simulation results show that only three features of the environment semantics can achieve almost the same accuracy as the whole environment semantics, which can significantly reduce system overheads and improve the transmission efficiency. The superiority of the environment semantics aided wireless communication framework in realizing extremely low-latency beam prediction and supporting ultra-reliable communication links demonstrates its great application potential in URLLCs.

## REFERENCES

- [1] C. E. Shannon and W. Weaver, "The mathematical theory of information," *Urbana: University of Illinois Press*, vol. 97, no. 6, pp. 128–164, 1949.
- [2] M. Thomas and A. T. Joy, *Elements of information theory*. Wiley-Interscience, 2006.
- [3] B. Wang, F. Gao, S. Jin, H. Lin, and G. Y. Li, "Spatial- and frequency-wideband effects in millimeter-wave massive MIMO systems," *IEEE Trans. Signal Process.*, vol. 66, no. 13, pp. 3393–3406, Jul. 2018.
- [4] B. Wang, F. Gao, S. Jin, H. Lin, G. Y. Li, S. Sun, and T. S. Rappaport, "Spatial-wideband effect in massive MIMO with application in mmwave systems," *IEEE Commun. Mag.*, vol. 56, no. 12, pp. 134–141, Dec. 2018.
- [5] Z. Qin, H. Ye, G. Y. Li, and B. F. Juang, "Deep learning in physical layer communications," *IEEE Wireless Commun.*, vol. 26, no. 2, pp. 93–99, Apr. 2019.
- [6] Q. Hu, F. Gao, H. Zhang, S. Jin, and G. Y. Li, "Deep learning for channel estimation: Interpretation, performance, and comparison," *IEEE Trans. Wireless Commun.*, vol. 20, no. 4, pp. 2398–2412, Dec. 2021.
- [7] H. He, C. Wen, S. Jin, and G. Y. Li, "Deep learning-based channel estimation for beamspace mmwave massive MIMO systems," *IEEE Wireless Commun. Lett.*, vol. 7, no. 5, pp. 852–855, Oct. 2018.
- [8] Y. Yang, F. Gao, G. Y. Li, and M. Jian, "Deep learning based downlink channel prediction for FDD massive MIMO system," *IEEE Commun. Lett.*, vol. 23, no. 11, pp. 1994–1998, Nov. 2019.
- [9] Y. Yang, F. Gao, Z. Zhong, B. Ai, and A. Alkhateeb, "Deep transfer learning based downlink channel prediction for FDD massive MIMO systems," *IEEE Trans. Commun.*, vol. 68, no. 12, pp. 7485–7497, Dec. 2020.
- [10] H. Ye, G. Y. Li, and B. Juang, "Power of deep learning for channel estimation and signal detection in OFDM systems," *IEEE Wireless Commun. Lett.*, vol. 7, no. 1, pp. 114–117, Feb. 2018.
- [11] Y. Yang, F. Gao, M. Wang, J. Xue, and Z. Xu, "Dynamic neural network for MIMO detection," *IEEE J. Selected Areas Commun.*, vol. 40, no. 8, pp. 2254–2266, Jun. 2022.
- [12] H. He, C. Wen, S. Jin, and G. Y. Li, "Model-driven deep learning for MIMO detection," *IEEE Trans. Signal Process.*, vol. 68, pp. 1702–1715, Feb. 2020.
- [13] T. Wang, C. Wen, S. Jin, and G. Y. Li, "Deep learning-based CSI feedback approach for time-varying massive MIMO channels," *IEEE Wireless Commun. Lett.*, vol. 8, no. 2, pp. 416–419, Apr. 2019.
- [14] J. Guo, C. Wen, S. Jin, and G. Y. Li, "Convolutional neural network based multiple-rate compressive sensing for massive MIMO CSI feedback: Design, simulation, and analysis," *IEEE Trans. Wireless Commun.*, vol. 19, no. 4, pp. 2827–2840, Apr. 2020.
- [15] J. Guo, J. Wang, C. Wen, S. Jin, and G. Y. Li, "Compression and acceleration of neural networks for communications," *IEEE Wireless Commun.*, vol. 27, no. 4, pp. 110–117, Aug. 2020.
- [16] J. Guo, C. Wen, and S. Jin, "Deep learning-based CSI feedback for beamforming in single- and multi-cell massive MIMO systems," *IEEE J. Selected Areas Commun.*, vol. 39, no. 7, pp. 1872–1884, Dec. 2021.
- [17] Z. Liu, Y. Yang, F. Gao, T. Zhou, and H. Ma, "Deep unsupervised learning for joint antenna selection and hybrid beamforming," *arXiv preprint arXiv:2106.03127*, 2021.
- [18] Q. Wang, K. Feng, X. Li, and S. Jin, "PrecoderNet: Hybrid beamforming for millimeter wave systems with deep reinforcement learning," *IEEE Wireless Commun. Lett.*, vol. 9, no. 10, pp. 1677–1681, Jun. 2020.
- [19] X. Luo, H.-H. Chen, and Q. Guo, "Semantic communications: Overview, open issues, and future research directions," *IEEE Wireless Commun.*, vol. 29, no. 1, pp. 210–219, Jan. 2022.
- [20] G. Shi, Y. Xiao, Y. Li, and X. Xie, "From semantic communication to semantic-aware networking: Model, architecture, and open problems," *IEEE Commun. Mag.*, vol. 59, no. 8, pp. 44–50, Sep. 2021.
- [21] M. Kalfa, M. Gok, A. Atalik, B. Tegin, T. M. Duman, and O. Arikan, "Towards goal-oriented semantic signal processing: Applications and future challenges," *Digit. Signal Process.*, vol. 119, no. C, Dec. 2021. [Online]. Available: <https://doi.org/10.1016/j.dsp.2021.103134>
- [22] M. Malik, M. K. Malik, K. Mehmood, and I. Makhdoom, "Automatic speech recognition: A survey," *Multimedia Tools Appl.*, vol. 80, no. 6, pp. 9411–9457, Mar. 2021. [Online]. Available: <https://doi.org/10.1007/s11042-020-10073-7>
- [23] H. Zhao, J. Shi, X. Qi, X. Wang, and J. Jia, "Pyramid scene parsing network," in *Proc. IEEE/CVF Conf. Comput. Vis. Pattern Recognit. (CVPR)*, Honolulu, USA, Jul. 2017, pp. 6230–6239.
- [24] D. Huang, X. Tao, C. Jiang, S. Cui, and J. Lu, "Trace-driven QoE-aware proactive caching for mobile video streaming in metropolis," *IEEE Trans. Wireless Commun.*, vol. 19, no. 1, pp. 62–76, Sep. 2020.
- [25] H. Xie, Z. Qin, G. Y. Li, and B. H. Juang, "Deep learning enabled semantic communication systems," *IEEE Trans. Signal Process.*, vol. 69, pp. 2663–2675, Apr. 2021.
- [26] Q. Zhou, R. Li, Z. Zhao, C. Peng, and H. Zhang, "Semantic communication with adaptive universal transformer," *IEEE Wireless Commun. Lett.*, vol. 11, no. 3, pp. 453–457, Dec. 2022.
- [27] Z. Weng and Z. Qin, "Semantic communication systems for speech transmission," *IEEE J. Selected Areas Commun.*, vol. 39, no. 8, pp. 2434–2444, 2021.
- [28] D. Huang, X. Tao, F. Gao, and J. Lu, "Deep learning-based image semantic coding for semantic communications," in *Proc. IEEE Global Commun. Conf. (GLOBECOM)*, Madrid, Spain, Dec. 2021, pp. 1–6.
- [29] A. Vaswani, N. Shazeer, N. Parmar, J. Uszkoreit, L. Jones, A. N. Gomez, L. Kaiser, and I. Polosukhin, "Attention is all you need," in *Proc. 31st Int. Conf. Neural Inf. Process. Syst. (NeurIPS)*, ser. NIPS'17. Red Hook, NY, USA: Curran Associates Inc., 2017, pp. 6000–6010.
- [30] W. Xu, F. Gao, S. Jin, and A. Alkhateeb, "3D scene based beam selection for mmwave communications," *IEEE Wireless Commun. Lett.*, vol. 9, no. 11, pp. 1850–1854, Jun. 2020.
- [31] W. Xu, F. Gao, J. Zhang, X. Tao, and A. Alkhateeb, "Deep learning based channel covariance matrix estimation with user location and scene images," *IEEE Trans. Commun.*, vol. 69, no. 12, pp. 8145–8158, Aug. 2021.
- [32] G. Charan, M. Alrabeiah, and A. Alkhateeb, "Vision-aided 6G wireless communications: Blockage prediction and proactive handoff," *IEEE Trans. Vehicular Technol.*, vol. 70, no. 10, pp. 10 193–10 208, Aug. 2021.
- [33] Y. Yang, F. Gao, C. Xing, J. An, and A. Alkhateeb, "Deep multimodal learning: Merging sensory data for massive MIMO channel prediction," *IEEE J. Selected Areas Commun.*, vol. 39, no. 7, pp. 1885–1898, Dec. 2021.
- [34] E. C. Strinati and S. Barbarossa, "6G networks: Beyond shannon towards semantic and goal-oriented communications," *Computer Networks*, vol. 190, p. 107930, 2021.
- [35] A. Alkhateeb, "DeepMIMO: A generic deep learning dataset for millimeter wave and massive MIMO applications," in *Proc. Inf. Theory and Applications Workshop (ITA)*, San Diego, CA, Feb. 2019, pp. 1–8.
- [36] H. Zhang, Y. Zhang, J. Cosmas, N. Jawad, W. Li, R. Muller, and T. Jiang, "mmwave indoor channel measurement campaign for 5G new radio indoor broadcasting," *IEEE Trans. Broadcasting*, vol. 68, no. 2, pp. 331–344, Jan. 2022.
- [37] K. He, X. Zhang, S. Ren, and J. Sun, "Deep residual learning for image recognition," in *Proc. IEEE/CVF Conf. Comput. Vis. Pattern Recognit. (CVPR)*, Las Vegas, USA, Jun. 2016, pp. 770–778.
- [38] D. Kingma and J. Ba, "Adam: A method for stochastic optimization," *arXiv preprint arXiv:1412.6980*, 2014.
- [39] A. Dosovitskiy, G. Ros, F. Codevilla, A. Lopez, and V. Koltun, "CARLA: An open urban driving simulator," in *Proc. 1st Annual Conf. Robot Learning*, 2017, pp. 1–16.
- [40] P. A. Lopez, M. Behrisch, L. Bieker-Walz, J. Erdmann, Y.-P. Flötteröd, R. Hilbrich, L. Lücken, J. Rummel, P. Wagner, and E. Wießner, "Microscopic traffic simulation using SUMO," in *Proc. IEEE Int. Conf. Intell. Transp. Syst.*, 2018. [Online]. Available: <https://elib.dlr.de/124092/>
- [41] B. Zhou, H. Zhao, X. Puig, T. Xiao, S. Fidler, A. Barriuso, and A. Torralba, "Semantic understanding of scenes through the ADE20K dataset," *Int. J. Comput. Vision*, vol. 127, no. 3, pp. 302–321, Mar. 2019.